

Learning Tensor Train Representation with Automatic Rank Determination from Incomplete Noisy Data

Le Xu, Lei Cheng, Ngai Wong, and Yik-Chung Wu

Abstract—Tensor train (TT) decomposition, a powerful tool for analysing multidimensional data, exhibits superior performance in many signal processing and machine learning tasks. However, existing methods for TT decomposition either require the knowledge of the true TT ranks, or extensive fine-tuning the balance between model complexity and representation accuracy. In this paper, a fully Bayesian treatment of TT decomposition is employed to enable automatic rank determination. In particular, theoretical evidence is established for adopting a Gaussian-product-Gamma prior to induce sparsity on the slices of the TT cores, so that the model complexity is automatically determined even under incomplete and noisy observed data. Based on the proposed probabilistic model, an efficient learning algorithm is derived under the variational inference framework. Simulation results on synthetic data show the success of the proposed model and algorithm on recovering the ground-truth TT structure from incomplete noisy data. Further experiments on real world data demonstrate the proposed algorithm performs better in image completion and image classification, compared to other existing TT decomposition algorithms.

Index Terms—Bayesian Inference, Rank Determination, Tensor Train, Tensor Completion

I. INTRODUCTION

RECENTLY, driven by the increasing demand for multidimensional big data analysis, tensor decomposition has come up as an emerging technique that shows superior performance in a variety of data analytic tasks, including image completion [1]–[4], classification [5]–[7], and neural network compression [8]–[10]. In particular, the tensor train (TT) decomposition has made remarkable success in the above-mentioned applications, owing to its particular algebraic format:

$$\begin{aligned} \mathcal{X}_{j_1 j_2 \dots j_D} &= \sum_{r_2=1}^{R_2} \dots \sum_{r_D=1}^{R_D} \mathcal{G}_{1,r_2,j_1}^{(1)} \mathcal{G}_{r_2,r_3,j_2}^{(2)} \\ &\quad \dots \mathcal{G}_{r_D,1,j_D}^{(D)} \\ &= \mathcal{G}_{:::,j_1}^{(1)} \mathcal{G}_{:::,j_2}^{(2)} \dots \mathcal{G}_{:::,j_D}^{(D)} \\ &\triangleq \lll \mathcal{G}^{(1)}, \mathcal{G}^{(2)}, \dots, \mathcal{G}^{(D)} \ggg_{j_1 j_2 \dots j_D}, \end{aligned} \quad (1)$$

where $\mathcal{X} \in \mathbb{R}^{J_1 \times \dots \times J_D}$ is a D -th order tensor. From the first line of (1), it is stated that the (j_1, j_2, \dots, j_D) -th element of the D -th order tensor can be expressed as a multiple summation

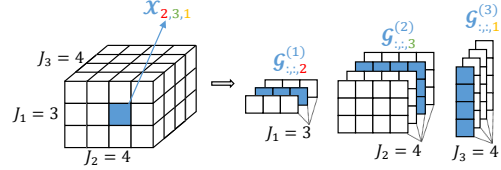


Fig. 1: An example of the tensor train decomposition.

of the product of elements from a number of 3-dimensional tensors $\{\mathcal{G}^{(d)} \in \mathbb{R}^{R_d \times R_{d+1} \times J_d}\}_{d=1}^D$, known as TT cores, with their size parameters $\{R_d\}_{d=1}^{D+1}$ termed as TT ranks (with R_1 and R_{D+1} fixed as 1). Furthermore, from the second line of (1), it can be seen that $\mathcal{X}_{j_1 j_2 \dots j_D}$ can also be interpreted as consecutive matrix products among frontal matrix slices in the TT cores. For the TT ranks $\{R_d\}_{d=1}^{D+1}$, they control the size of TT cores, and thus are deemed as the hyper-parameters that controls the model complexity. An example of the TT decomposition of a 3-dimensional tensor is illustrated in Fig. 1. In particular, $\mathcal{X}_{2,3,1} = \mathcal{G}_{:::,2}^{(1)} \mathcal{G}_{:::,3}^{(2)} \mathcal{G}_{:::,1}^{(3)}$ is highlighted in the figure, where the associated matrix slice index in the d -th TT core is the same as the d -th index of $\mathcal{X}_{2,3,1}$.

Consequently, the goal of TT representation is to learn 3-dimensional tensor cores $\{\mathcal{G}^{(d)}\}_{d=1}^D$ from the D -dimensional tensor data \mathcal{Y} , with the following optimization problem [11]–[15]:

$$\min_{\mathcal{G}^{(1)}, \mathcal{G}^{(2)}, \dots, \mathcal{G}^{(D)}} \left\| \mathcal{O} \circ \left(\mathcal{Y} - \lll \mathcal{G}^{(1)}, \mathcal{G}^{(2)}, \dots, \mathcal{G}^{(D)} \ggg \right) \right\|_F^2, \quad (2)$$

where \circ denotes element-by-element multiplication, and \mathcal{O} is the observation tensor with its element being 1 if the corresponding data element is observed and 0 otherwise. A number of algorithms have been put forward to solve special cases of (2) from the perspective of multi-linear algebra and optimization. For example, if the tensor is fully observed, TT-SVD [11] finds the TT cores based on truncated SVDs to the unfolding data matrices of tensor \mathcal{Y} . Although simple to implement, it cannot handle missing data in \mathcal{Y} , and is prone to overfitting of noises when the required reconstruction accuracy is set too high. On the other hand, when a tensor is not fully observed, alternating optimization methods, which update one TT-core in each iteration while keeping others fixed, are often adopted [12]–[15]. However, these methods require the knowledge of TT structure, or TT ranks explicitly, which unfortunately is unknown in practice. To bypass the challenge

Le Xu, Ngai Wong and Yik-Chung Wu are with the Department of Electrical and Electronic Engineering, The University of Hong Kong, Hong Kong, (email: xule@eee.hku.hk, nwong@eee.hku.hk, ycwu@eee.hku.hk).

Lei Cheng is with the Shenzhen Research Institute of Big Data, Shenzhen, Guangdong, P. R. China, (email: leicheng@sribd.cn).

of presetting TT ranks, recent works [2], [16] proposed a low-rank pursuing scheme, which targets at minimizing the weighted TT ranks, or incorporates the optimization of the TT ranks in a regularization term. While the tensor structure is not a prerequisite anymore, these schemes require fine-tuning the weightings in the objective function or regularization parameters, which may take different values under different applications, thus being very time-consuming in finding the right set of parameters. By far, identifying ranks in a TT model is still considered a challenge.

Identifying tensor ranks in other tensor decompositions is not new. For example, in the tensor canonical polyadic decomposition (CPD), the problem of finding the ranks has been well solved under the framework of Bayesian modeling and inference [3], [17], [18]. However, models from CPD cannot be straightforwardly extended to the TT format because of TT's unique algebraic structure in the coupling of adjacent TT cores through the ranks. We might draw some inspirations from Bayesian Tucker Decomposition (TD) [18], where the ranks of different factor matrices are coupled in the central core tensor.

In particular, going along with the modeling in Bayesian TD, we adopt a Gaussian-product-Gamma prior for the TT slices, where the variance of each element of the TT cores is determined by two hyper Gamma distributed parameters. While previous works using similar model demonstrate automatic rank selection experimentally [18], [19], it is proved in this paper for the first time that such model could theoretically lead to sparsity in TT slices, thus establishing the legitimacy of such modeling. After setting up the model for probabilistic TT decomposition, variational inference is adopted to approximate posterior distribution of the unknown parameters. Numerical experiments using both synthetic and real-world data show the superiority of the proposed model and the inference algorithm.

The rest of the paper is organized as follows. Section II introduces the Gaussian-product-Gamma distribution and how it is adopted in the TT model. The inference algorithm is introduced in Section III. Numerical results are presented in Section IV, and the conclusions are drawn in Section V.

Notation: In this paper, boldface lowercase and uppercase letters are used to denote vectors and matrices, respectively. Boldface capital calligraphic letters are used for tensors. \mathbf{I}_n denotes the identity matrix with size $n \times n$. $\mathbb{E}[\cdot]$ represents the expectation of the variables. $\mathcal{N}(\boldsymbol{\mu}, \boldsymbol{\Sigma})$ denotes the Gaussian distribution with mean $\boldsymbol{\mu}$ and variance $\boldsymbol{\Sigma}$, and $\text{Gamma}(\alpha, \beta)$ denotes the Gamma distribution with shape α and rate β . The operator \otimes denotes the kronecker product, and \circ denotes the entry-wise product of two tensors with the same size. Notation $\text{diag}(\mathbf{a})$ is a diagonal matrix, with \mathbf{a} on its diagonal. An element of a matrix or tensor is specified by the subscript, e.g. $\mathcal{Y}_{i,j,k}$ denotes the (i, j, k) -th element of tensor \mathcal{Y} , while $\mathcal{Y}_{:, :, k}$ includes all elements in the first and second modes with k fixed at the third mode.

II. PROBABILISTIC MODEL FOR TENSOR TRAIN REPRESENTATION

A. Sparsity Enhancing Probabilistic Modeling

The Gaussian-Gamma distribution is commonly used to induce sparsity in Bayesian modeling. For example, in matrix factorization [20] and tensor CPD [3], [17], the rank-1 components are assigned with zero-mean Gaussian distributions, with their precisions being modeled as Gamma random variables. The sparsity promoting character of the Gaussian-Gamma distribution guarantees that the unimportant components can be easily recognized and thus be discarded automatically [18], [21]. However, this model is not suitable for the TT decomposition, since matrix factorization or tensor CPD is only controlled by a single rank, while TT decomposition consists of multiple ranks with each rank constraining the dimensions of two adjacent TT cores. To extend the Gaussian-Gamma distribution to model coupling, we could employ a strategy similar to Bayesian Tucker model [18], in which the precisions of the coupled components are multiplied together, leading to the following Gaussian-product-Gamma model:

$$\begin{aligned} p(x|\lambda_1, \lambda_2) &= \mathcal{N}(x|0, (\lambda_1\lambda_2)^{-1}), \\ p(\lambda_1) &= \text{Gamma}(\lambda_1|\alpha_1, \beta_1), \quad p(\lambda_2) = \text{Gamma}(\lambda_2|\alpha_2, \beta_2), \end{aligned} \quad (3)$$

where Gamma variables λ_1 and λ_2 jointly determine the precision of the Gaussian variable x . Although empirically shown to be effective in rank selection [18], [19], the effect of the product of precision parameters on the Gaussian-Gamma prior pair has never been theoretically analyzed. To gain more insights into the model in (3), we present the following two properties.

Property 1. The Gamma distribution is conditionally conjugate to the Gaussian distribution in (3). That is,

$$p(\lambda_1|x, \lambda_2, \alpha_1, \beta_1, \alpha_2, \beta_2) = \text{Gamma}(\lambda_1|\alpha_1 + \frac{1}{2}, \frac{\lambda_2}{2}x^2 + \beta_1), \quad (4)$$

and a similar result holds for λ_2 . While (4) is not the full conjugate property, it still ensures a closed-form update in the inference procedure.

Proof: See Appendix A.

Property 2. The Gaussian-product-Gamma model in (3) is sparsity promoting. The marginal distribution of x is given by:

$$\begin{aligned} p(x|\alpha_1, \beta_1, \alpha_2, \beta_2) &= \frac{\beta_1^{\alpha_1} \beta_2^{\alpha_2} \Gamma(\alpha_1 + \frac{1}{2})}{\sqrt{2\pi} \Gamma(\alpha_1) \Gamma(\alpha_2)} \int \exp\{-\beta_2 \lambda_2\} \\ &\quad \lambda_2^{\alpha_2 - \frac{1}{2}} \left(\frac{(\sqrt{\lambda_2} x)^2}{2} + \beta_1 \right)^{-(\alpha_1 + \frac{1}{2})} d\lambda_2. \end{aligned} \quad (5)$$

Proof: See Appendix A.

The integration in (5) can be seen as an infinite mixture of student-t distributions [22, p. 103], in which the variable x is scaled by $\sqrt{\lambda_2}$, and the mixing parameter λ_2 follows a Gamma distribution. Thus the marginal distribution would peak at zero, similar to the student-t distribution. Especially, when $\alpha_1, \alpha_2, \beta_1, \beta_2$ all tend to zero, $(\frac{(\sqrt{\lambda_2} x)^2}{2} + \beta_1)^{-(\alpha_1 + \frac{1}{2})}$ in

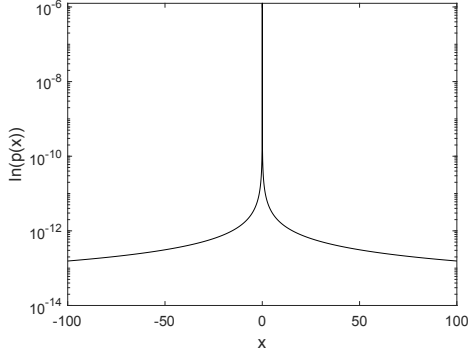


Fig. 2: Marginal distribution (5) with $\alpha_1 = \alpha_2 = 10^{-6}$, $\beta_1 = \beta_2 = 10^{-6}$.

(5) would tend to $\sqrt{\frac{2}{\lambda_2} \frac{1}{|x|}}$, thus the marginal distribution of x will be proportional to $\frac{1}{|x|}$, which highly peaks at zero and has a heavy tail. Fig. 2 illustrates the marginal distribution of x with numerical integration of (5) when $\alpha_1 = \alpha_2 = 10^{-6}$, $\beta_1 = \beta_2 = 10^{-6}$.

B. Likelihood and Priors for the Tensor Train Model

The observed tensor can be expressed as

$$\mathcal{A} = \mathcal{O} \circ (\mathcal{Y} + \mathcal{W}), \quad (6)$$

where $\mathcal{Y} = \ll \mathcal{G}^{(1)}, \mathcal{G}^{(2)}, \dots, \mathcal{G}^{(D)} \gg$ is the ground-truth tensor which is assumed to be in the TT format, and \mathcal{W} is a noise tensor, with each element modeled as independent and identically distributed (i.i.d.) Gaussian variables with mean 0 and precision τ (i.e., the inverse of the variance). Correspondingly, the logarithm of the likelihood function of the observed tensor is

$$\begin{aligned} & \ln \left(p(\mathcal{A} | \mathcal{O}, \{\mathcal{G}^{(d)}\}_{d=1}^D, \tau) \right) \\ &= \sum_{\{j_1, j_2, \dots, j_D\} \in \Omega} \ln \mathcal{N}(\mathcal{A}_{j_1, \dots, j_D} | \mathcal{G}_{:, :, j_1}^{(1)} \mathcal{G}_{:, :, j_2}^{(2)} \dots \mathcal{G}_{:, :, j_D}^{(D)}, \tau^{-1}) \\ &= \frac{|\Omega|}{2} \ln \tau - \frac{\tau}{2} \left\| \mathcal{O} \circ (\mathcal{A} - \ll \mathcal{G}^{(1)}, \mathcal{G}^{(2)}, \dots, \mathcal{G}^{(D)} \gg) \right\|_F^2 \\ & \quad + \text{const}, \end{aligned} \quad (7)$$

where Ω denotes the set of indices of the observed entries, and $|\Omega|$ denotes the cardinality of Ω , which equals the number of observed entries. It is not difficult to see that the result of maximizing (7) will be the same as that of solving problem (2), regardless what the noise variance τ^{-1} is. However, as discussed in the last section, minimizing the square error works well only when the tensor train ranks are suitably chosen. Thus, instead of maximizing the log-likelihood, we build a hierarchical probabilistic model by treating $\{\mathcal{G}^{(d)}\}_{d=1}^D$ as variables, which enhances the expressive power of the model, and allows automatic rank determination. As has been discussed in the last sub-section, the Gaussian-product-Gamma

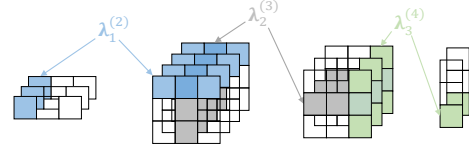


Fig. 3: Coupling of $\{\lambda^{(d)}\}$ in the TT model.

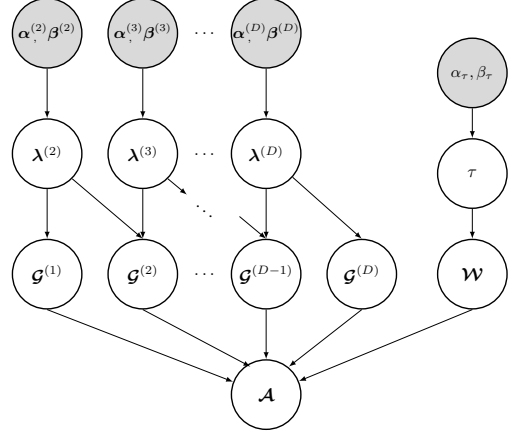


Fig. 4: Probabilistic model for the TT decomposition.

prior (3) can be adopted for the TT cores to induce sparsity:

$$\begin{aligned} & p(\mathcal{G}^{(d)} | \lambda^{(d)}, \lambda^{(d+1)}) \\ &= \prod_{k=1}^{L_d} \prod_{\ell=1}^{L_{d+1}} \mathcal{N} \left(\mathcal{G}_{k, \ell, :}^{(d)} | \mathbf{0}, (\lambda_k^{(d)} \lambda_\ell^{(d+1)})^{-1} \mathbf{I}_{J_d} \right), \quad (8) \\ & \quad \forall d \in \{1, 2, \dots, D\}, \end{aligned}$$

$$\begin{aligned} & p(\lambda^{(d)} | \alpha^{(d)}, \beta^{(d)}) \\ &= \prod_{k=1}^{L_d} \text{Gamma}(\lambda_k^{(d)} | \alpha_k^{(d)}, \beta_k^{(d)}), \quad \forall d \in \{2, \dots, D\}, \quad (9) \end{aligned}$$

where $\lambda^{(d)} = [\lambda_1^{(d)}, \dots, \lambda_{L_d}^{(d)}]$ for $d = 2, \dots, D$, $\lambda^{(1)}$ and $\lambda^{(D+1)}$ are scalars and set as 1 so that the expression in (8) is applicable for the first and last TT cores. Furthermore, $\alpha^{(d)} = [\alpha_1^{(d)}, \dots, \alpha_{L_d}^{(d)}]$ and $\beta^{(d)} = [\beta_1^{(d)}, \dots, \beta_{L_d}^{(d)}]$ for $d = 2, \dots, D$ are hyperparameters of the Gamma distributions, with $\text{Gamma}(x | \alpha, \beta) = \beta^\alpha x^{\alpha-1} e^{-\beta x} / \Gamma(\alpha)$. In (8) and (9), $\{L_d\}_{d=1}^D$ are the assumed TT ranks, which are chosen as large numbers such that automatic selection of important tensor core slices $\mathcal{G}_{k, :, :}^{(d)}$ or $\mathcal{G}_{:, \ell, :}^{(d)}$ is possible during model inference. A simple demonstration of the coupling in (8) is depicted in Fig. 3.

Notice that the Gaussian-product-Gamma prior for the TT cores is more complicated than that in (3) since the $\lambda_k^{(d)}$ in (8) and (9) controls the k -th lateral slice of $\mathcal{G}^{(d-1)}$ and the k -th horizontal slice of $\mathcal{G}^{(d)}$, while λ_1 in (3) only controls a univariate x . Although with the difference, the sparsity promoting property still exists as follows, thus facilitating rank selection.

Property 3. The Gaussian-product-Gamma model in (8) and (9) would induce sparsity in all lateral and horizontal slices of the TT cores.

Proof: See Appendix B.

Finally, for the noise precision, we model it as a Gamma distribution with hyperparameters α_τ and β_τ :

$$p(\tau|\alpha_\tau, \beta_\tau) = \text{Gamma}(\tau|\alpha_\tau, \beta_\tau). \quad (10)$$

Since we have no information about the distribution of $\{\boldsymbol{\lambda}^{(d)}\}$ and τ , we set $\boldsymbol{\alpha}^{(d)} = \boldsymbol{\beta}^{(d)} = 10^{-6} \times \mathbf{1}_{L_d \times 1}$ and $\alpha_\tau = \beta_\tau = 10^{-6}$ to make (9) and (10) non-informative. The hierarchical probabilistic model for the TT decomposition is shown in Fig. 4.

III. INFERENCE ALGORITHM

The goal of Bayesian inference is to find the posterior distribution of the unknown variables $\Theta := \{\{\boldsymbol{g}^{(d)}\}_{d=1}^D, \{\boldsymbol{\lambda}^{(d)}\}_{d=2}^D, \tau\}$, and subsequently the marginal distribution of each of the variables. First of all, the logarithm of the joint distribution $\ln(p(\mathcal{A}, \Theta))$ is obtained by summing the logarithm of the priors (8), (9), (10) and the log-likelihood (7):

$$\begin{aligned} \ln(p(\mathcal{A}, \Theta)) &= \frac{|\Omega|}{2} \ln \tau - \frac{\tau}{2} \left\| \mathcal{O} \circ (\mathcal{A} - \ll \boldsymbol{g}^{(1)}, \boldsymbol{g}^{(2)}, \dots, \boldsymbol{g}^{(D)} \gg) \right\|_F^2 \\ &+ \frac{1}{2} \sum_{d=1}^D \sum_k^{L_d} \sum_\ell^{L_{d+1}} \left(J_d \ln(\lambda_k^{(d)} \lambda_\ell^{(d+1)}) - \lambda_k^{(d)} \lambda_\ell^{(d+1)} \right. \\ &\quad \left. \sum_{j_d=1}^{J_d} \boldsymbol{g}_{k,\ell,j_d}^{(d)2} \right) + \sum_{d=2}^D \sum_{k=1}^{L_d} \left((\alpha_k^{(d)} - 1) \ln \lambda_k^{(d)} - \beta_k^{(d)} \lambda_k^{(d)} \right) \\ &+ (\alpha_\tau - 1) \ln \tau - \beta_\tau \tau + \text{const.} \end{aligned} \quad (11)$$

From (11), it can be seen that the posterior distribution $p(\Theta|\mathcal{A}) = p(\mathcal{A}, \Theta)/p(\mathcal{A})$ is intractable due to the coupling of variables, which makes computing $p(\mathcal{A}) = \int p(\mathcal{A}, \Theta) d\Theta$ difficult. To bypass this problem, we turn to variational inference (VI), which uses a variational distribution $q(\Theta)$ to approximate the true posterior $p(\Theta|\mathcal{A})$, by minimizing their Kullback-Leibler (KL) divergence:

$$\min_{q(\Theta)} \text{KL} \left(q(\Theta) \parallel p(\Theta|\mathcal{A}) \right) = \int q(\Theta) \ln \frac{q(\Theta)}{p(\Theta|\mathcal{A})} d\Theta. \quad (12)$$

Mean-field approximation $q(\Theta) = \prod_s^S q(\Theta_s)$ with $\Theta_s \subset \Theta$, $\cup_{s=1}^S \Theta_s = \Theta$, and $\Theta_s \cap \Theta_t = \emptyset$ for $s \neq t$, is commonly adopted to simplify (12). Under this approximation, the optimal variational distribution of each variable set Θ_s can be obtained as [23, pp. 737]:

$$\ln q^*(\Theta_s) = \mathbb{E}_{\Theta \setminus \Theta_s} [\ln p(\mathcal{A}, \Theta)] + \text{const}, \quad (13)$$

where $\mathbb{E}_{\Theta \setminus \Theta_s}$ means expectation with respect to Θ except Θ_s . It is obvious that when computing for $q^*(\Theta_s)$, we need to know $q(\Theta_t)$ where $t \neq s$. Therefore, the variational distribution needs to be updated iteratively for different s . Since (13) is a convex problem with respect to each $q(\Theta_s)$ [22, pp. 466], the convergence of the iterative updating procedure is guaranteed.

For the proposed TT model, we impose the mean-field approximation as $q(\Theta) = q(\tau) \prod_{d=1}^{D+1} q(\boldsymbol{\lambda}^{(d)})$

$\prod_{d=1}^D \prod_{k=1}^{L_d} \prod_{\ell=1}^{L_{d+1}} q(\boldsymbol{g}_{k,\ell,:}^{(d)})$, and the optimal variational distribution at each iteration is derived next.

Updating $q(\boldsymbol{g}_{k,\ell,:}^{(d)})$

for $d \in \{1, \dots, D\}$, $k \in \{1, \dots, L_d\}$, $\ell \in \{1, \dots, L_{d+1}\}$

$$\begin{aligned} &\text{Substituting (11) into (13) with } \Theta_s \text{ set as } \boldsymbol{g}_{k,\ell,:}^{(d)}, \text{ we obtain} \\ \ln q(\boldsymbol{g}_{k,\ell,:}^{(d)}) &= \mathbb{E}_{\Theta \setminus \boldsymbol{g}_{k,\ell,:}^{(d)}} \left[-\frac{\tau}{2} \left\| \mathcal{O} \circ (\mathcal{A} - \ll \boldsymbol{g}^{(1)}, \boldsymbol{g}^{(2)}, \dots, \boldsymbol{g}^{(D)} \gg) \right\|_F^2 \right. \\ &\quad \left. - \frac{1}{2} \lambda_k^{(d)} \lambda_\ell^{(d+1)} \sum_{j_d=1}^{J_d} \boldsymbol{g}_{k,\ell,j_d}^{(d)2} \right] + \text{const.} \end{aligned} \quad (14)$$

For the Frobenius norm, it can be expanded as

$$\begin{aligned} &\left\| \mathcal{O} \circ (\mathcal{A} - \ll \boldsymbol{g}^{(1)}, \boldsymbol{g}^{(2)}, \dots, \boldsymbol{g}^{(D)} \gg) \right\|_F^2 \\ &= \sum_{j_1=1}^{J_1} \dots \sum_{j_D=1}^{J_D} \left(\mathcal{O}_{j_1 \dots j_D} \left(-2 \mathcal{A}_{j_1 \dots j_D} \boldsymbol{g}_{:,j_1}^{(1)} \dots \boldsymbol{g}_{:,j_D}^{(D)} \right. \right. \\ &\quad \left. \left. + (\boldsymbol{g}_{:,j_1}^{(1)} \dots \boldsymbol{g}_{:,j_D}^{(D)})^2 \right) \right)^2 + \text{const.} \end{aligned} \quad (15)$$

As shown in (14), the expectation is taken over all variables except $\boldsymbol{g}_{k,\ell,:}^{(d)}$. The difficulty comes from the second order term $(\boldsymbol{g}_{:,j_1}^{(1)} \dots \boldsymbol{g}_{:,j_D}^{(D)})^2$, since the slices of different TT cores are multiplied and then squared. Fortunately, notice that $(\boldsymbol{g}_{:,j_1}^{(1)} \dots \boldsymbol{g}_{:,j_D}^{(D)})^2$ is a scalar and thus can be written as $(\boldsymbol{g}_{:,j_1}^{(1)} \dots \boldsymbol{g}_{:,j_D}^{(D)}) \otimes (\boldsymbol{g}_{:,j_1}^{(1)} \dots \boldsymbol{g}_{:,j_D}^{(D)})$. Using the mixed-product property of the Kronecker product $(\mathcal{A}_1 \dots \mathcal{A}_D) \otimes (\mathcal{B}_1 \dots \mathcal{B}_D) = (\mathcal{A}_1 \otimes \mathcal{B}_1) \dots (\mathcal{A}_D \otimes \mathcal{B}_D)$, $(\boldsymbol{g}_{:,j_1}^{(1)} \dots \boldsymbol{g}_{:,j_D}^{(D)})^2$ can be further expressed as $\prod_{d=1}^D (\boldsymbol{g}_{:,j_d}^{(d)} \otimes \boldsymbol{g}_{:,j_d}^{(d)})$. By substituting this result into (15), $\ln(\boldsymbol{g}_{k,\ell,:}^{(d)})$ can be obtained as

$$\begin{aligned} \ln q(\boldsymbol{g}_{k,\ell,:}^{(d)}) &= \sum_{j_d=1}^{J_d} \mathbb{E}_{\Theta \setminus \boldsymbol{g}_{k,\ell,:}^{(d)}} \left[-\frac{\tau}{2} \sum_{j_1, \dots, j_D \setminus j_d} \left(\mathcal{O}_{j_1 \dots j_D} \left(-2 \mathcal{A}_{j_1 \dots j_D} \right. \right. \right. \\ &\quad \underbrace{\boldsymbol{g}_{:,j_1}^{(1)} \dots \boldsymbol{g}_{:,j_d}^{(d)}}_{\boldsymbol{t}(<d)^T} \dots \underbrace{\boldsymbol{g}_{:,j_d}^{(d)} \dots \boldsymbol{g}_{:,j_D}^{(D)}}_{\boldsymbol{t}(>d)} + \underbrace{(\boldsymbol{g}_{:,j_1}^{(1)} \otimes \boldsymbol{g}_{:,j_1}^{(1)}) \dots}_{\boldsymbol{b}(<d)^T} \\ &\quad \left. \left. \left. (\boldsymbol{g}_{:,j_d}^{(d)} \otimes \boldsymbol{g}_{:,j_d}^{(d)}) \dots \underbrace{(\boldsymbol{g}_{:,j_D}^{(D)} \otimes \boldsymbol{g}_{:,j_D}^{(D)})}_{\boldsymbol{b}(>d)} \right) \right)^2 \right] \\ &\quad \left. - \frac{1}{2} \lambda_k^{(d)} \lambda_\ell^{(d+1)} \boldsymbol{g}_{k,\ell,j_d}^{(d)2} \right] + \text{const.} \end{aligned} \quad (16)$$

It is noticed that (16) is a quadratic function of $\boldsymbol{g}_{k,\ell,:}^{(d)}$, so $q(\boldsymbol{g}_{k,\ell,:}^{(d)})$ must follow a Gaussian distribution. Moreover, it can be seen that the elements indexed by different j_d are independent of each other, and thus can be updated separately. Therefore, $q(\boldsymbol{g}_{k,\ell,:}^{(d)}) = \prod_{j_d=1}^{J_d} \mathcal{N}(m_{\boldsymbol{g}_{k,\ell,j_d}^{(d)}}, \nu_{\boldsymbol{g}_{k,\ell,j_d}^{(d)}})$ with the

mean and variance given by

$$m_{\mathcal{G}_{k,\ell,j_d}^{(d)}} = v_{\mathcal{G}_{k,\ell,j_d}^{(d)}} \langle \tau \rangle \sum_{j_1, j_2, \dots, j_D \setminus j_d} \mathcal{O}_{j_1 j_2 \dots j_D} \left(\mathcal{A}_{j_1 j_2 \dots j_D} \right. \\ \left. \langle \mathbf{t}_k^{(<d)} \rangle \langle \mathbf{t}_\ell^{(>d)} \rangle - \sum_{\substack{k'=1 \\ k' \neq k}}^{L_d} \sum_{\substack{\ell'=1 \\ \ell' \neq \ell}}^{L_{d+1}} \langle \mathbf{b}_{(k-1)L_d+k'}^{(<d)} \rangle \right. \\ \left. \langle \mathcal{G}_{k',\ell',j_d}^{(d)} \rangle \langle \mathbf{b}_{(\ell-1)L_{d+1}+\ell'}^{(>d)} \rangle \right), \quad (17)$$

$$v_{\mathcal{G}_{k,\ell,j_d}^{(d)}} = \left(\langle \tau \rangle \sum_{j_1, j_2, \dots, j_D \setminus j_d} \mathcal{O}_{j_1 j_2 \dots j_D} \langle \mathbf{b}_{(k-1)L_d+k}^{(<d)} \rangle \right. \\ \left. \langle \mathbf{b}_{(\ell-1)L_{d+1}+\ell}^{(>d)} \rangle + \langle \lambda_k^{(d)} \rangle \langle \lambda_\ell^{(d+1)} \rangle \right)^{-1}, \quad (18)$$

where $\langle x \rangle$ denotes the expectation of the variable x with respect to $q(x)$. As can be seen from (18), the variance of the TT cores is affected by $\{\lambda^{(d)}\}_{d=2}^D$. If $\lambda_k^{(d)}$ is large enough, the variance of all elements in both slices $\mathcal{G}_{:,k,:}^{(d)}$ and $\mathcal{G}_{k,:}^{(d+1)}$ will tend to zero. Moreover, (17) shows that a small variance will further force the mean of a slice to be zero, and in such a way $\{\lambda^{(d)}\}$ contributes to rank selection.

Since different cores are assumed to be independent in the mean-field approximation, we obtain $\langle \mathbf{t}^{(<d)} \rangle = \langle \mathcal{G}_{:,j_1}^{(1)} \rangle \dots \langle \mathcal{G}_{:,j_{d-1}}^{(d-1)} \rangle$ and $\langle \mathbf{b}^{(>d)} \rangle = \langle \mathcal{G}_{:,j_1}^{(1)} \otimes \mathcal{G}_{:,j_1}^{(1)} \rangle \dots \langle \mathcal{G}_{:,j_{d-1}}^{(d-1)} \otimes \mathcal{G}_{:,j_{d-1}}^{(d-1)} \rangle$, and similar results hold for $\mathbf{t}^{(>d)}$ and $\mathbf{b}^{(>d)}$. For the expectation of the TT core $\langle \mathcal{G}_{:,j_e}^{(e)} \rangle$, since $\mathcal{G}_{:,j_e}^{(e)}$ follows a Gaussian distribution, we take $\langle \mathcal{G}_{:,j_e}^{(e)} \rangle = m_{\mathcal{G}_{:,j_e}^{(e)}}$. For the expectation of $\mathcal{G}_{:,j_e}^{(e)} \otimes \mathcal{G}_{:,j_e}^{(e)}$, it can be calculated by

$$\langle \mathcal{G}_{:,j_e}^{(e)} \otimes \mathcal{G}_{:,j_e}^{(e)} \rangle = \langle \mathcal{G}_{:,j_e}^{(e)} \rangle \otimes \langle \mathcal{G}_{:,j_e}^{(e)} \rangle + \mathcal{V}_{:,j_e}^{(e)}, \quad (19)$$

where $\mathcal{V}_{:,j_e}^{(e)} = \langle (\mathcal{G}_{:,j_e}^{(e)} - \langle \mathcal{G}_{:,j_e}^{(e)} \rangle) \otimes (\mathcal{G}_{:,j_e}^{(e)} - \langle \mathcal{G}_{:,j_e}^{(e)} \rangle) \rangle$ is the Kronecker-form covariance. Because $q(\mathcal{G}^{(e)}) = \prod_{k=1}^{L_e} \prod_{\ell=1}^{L_{e+1}} q(\mathcal{G}_{k,\ell,:}^{(e)})$ is assumed in the mean-field, $\langle (\mathcal{G}_{k,\ell,j_e}^{(e)} - m_{\mathcal{G}_{k,\ell,j_e}^{(e)}}) (\mathcal{G}_{k',\ell',j_e}^{(e)} - m_{\mathcal{G}_{k',\ell',j_e}^{(e)}}) \rangle = v_{\mathcal{G}_{k,\ell,j_e}^{(e)}} \delta(k-k') \delta(\ell-\ell')$, where $\delta(x) = 1$ if $x = 0$ and zero otherwise. Therefore, $\mathcal{V}_{:,j_e}^{(e)} \in \mathbb{R}^{L_d^2 \times L_{d+1}^2}$ consists of block matrices with dimension $L_d \times L_{d+1}$ and the (k, ℓ) -th block matrix contains only one nonzero element $v_{\mathcal{G}_{k,\ell,j_e}^{(e)}}$ at the (k, ℓ) -th position.

Updating $q(\lambda^{(d)})$ for $d \in \{2, \dots, D\}$

The update for $q(\lambda^{(d)})$ is calculated by substituting (11) into (13) with Θ_s set as $\lambda^{(d)}$:

$$\ln q(\lambda^{(d)}) = \sum_{k=1}^{L_d} \left[\mathbb{E}_{\Theta \setminus \lambda^{(d)}} \left[\ln \lambda_k^{(d)} \left(\frac{J_d L_{d+1}}{2} \right. \right. \right. \\ \left. \left. \left. + \frac{J_{d-1} L_{d-1}}{2} + \alpha_k^{(d)} - 1 \right) - \left(\frac{1}{2} \sum_{j_d=1}^{J_d} \sum_{\ell=1}^{L_{d+1}} \mathcal{G}_{k,\ell,j_d}^{(d)} \lambda_\ell^{(d+1)} \right. \right. \right. \\ \left. \left. \left. + \frac{1}{2} \sum_{j_{d-1}=1}^{J_{d-1}} \sum_{\ell'=1}^{L_{d-1}} \mathcal{G}_{\ell',k,j_{d-1}}^{(d-1)} \lambda_{\ell'}^{(d-1)} + \beta_k^{(d)} \right) \lambda_k^{(d)} \right] \right] + \text{const.} \quad (20)$$

From (20) it is not hard to see that $q(\lambda^{(d)}) = \prod_{k=1}^{L_d} \text{Gamma}(\lambda_k^{(d)} | \hat{\alpha}_k^{(d)}, \hat{\beta}_k^{(d)})$ with parameters

$$\hat{\alpha}_k^{(d)} = \frac{J_d L_{d-1}}{2} + \frac{J_{d-1} L_{d-1}}{2} + \alpha_k^{(d)}, \quad (21)$$

$$\hat{\beta}_k^{(d)} = \frac{1}{2} \sum_{j_d=1}^{J_d} \sum_{\ell=1}^{L_{d+1}} (\langle \mathcal{G}_{k,\ell,j_d}^{(d)} \rangle^2 \langle \lambda_\ell^{(d+1)} \rangle) \\ + \frac{1}{2} \sum_{j_{d-1}=1}^{J_{d-1}} \sum_{\ell'=1}^{L_{d-1}} (\langle \mathcal{G}_{\ell',k,j_{d-1}}^{(d-1)} \rangle^2 \langle \lambda_{\ell'}^{(d-1)} \rangle) + \beta_k^{(d)}, \quad (22)$$

in which $\langle \mathcal{G}_{k,\ell,j_d}^{(d)} \rangle^2$ can be obtained by picking up the $(kL_d + k, \ell L_{d+1} + \ell)$ -th element from $\langle \mathcal{G}_{:,j_e}^{(e)} \otimes \mathcal{G}_{:,j_e}^{(e)} \rangle$ in (19), and $\langle \lambda_\ell^{(d)} \rangle = \hat{\alpha}_\ell^{(d)} / \hat{\beta}_\ell^{(d)}$ according to the property of the Gamma distribution [24, pp. 70].

Updating $q(\tau)$

To obtain the distribution update for τ , we compute

$$\ln q(\tau) \\ = \mathbb{E}_{\Theta \setminus \tau} \left[\left(-\frac{1}{2} (\|\mathcal{O} \circ \mathcal{A}\|_F^2 - 2 \sum_{j_1=1}^{J_1} \dots \sum_{j_D=1}^{J_D} \mathcal{O}_{j_1 \dots j_D}) \right. \right. \\ \left. \left. \times \mathcal{A}_{j_1 \dots j_D} \prod_{d=1}^D \mathcal{G}_{:,j_d}^{(d)} + \sum_{j_1=1}^{J_1} \dots \sum_{j_D=1}^{J_D} \mathcal{O}_{j_1 \dots j_D} \right. \right. \\ \left. \left. \times \prod_{d=1}^D \mathcal{G}_{:,j_d}^{(d)} \otimes \mathcal{G}_{:,j_d}^{(d)} - \beta_\tau \right) \tau + \left(\frac{|\Omega|}{2} + \alpha_\tau - 1 \right) \ln \tau \right] \\ + \text{const}, \quad (23)$$

which clearly shows that τ obeys a Gamma distribution, with parameters

$$\hat{\alpha}_\tau = \frac{|\Omega|}{2} + \alpha_\tau, \quad (24)$$

$$\hat{\beta}_\tau = \frac{1}{2} \left(\|\mathcal{O} \circ \mathcal{A}\|_F^2 - 2 \sum_{j_1=1}^{J_1} \dots \sum_{j_D=1}^{J_D} \mathcal{O}_{j_1 \dots j_D} \mathcal{A}_{j_1 \dots j_D} \right. \\ \left. \times \prod_{d=1}^D \langle \mathcal{G}_{:,j_d}^{(d)} \rangle + \sum_{j_1=1}^{J_1} \dots \sum_{j_D=1}^{J_D} \mathcal{O}_{j_1 \dots j_D} \right. \\ \left. \times \prod_{d=1}^D \langle \mathcal{G}_{:,j_d}^{(d)} \otimes \mathcal{G}_{:,j_d}^{(d)} \rangle \right) \beta_\tau. \quad (25)$$

The calculation of $\langle \mathcal{G}_{:,j_d}^{(d)} \rangle$ and $\langle \mathcal{G}_{:,j_d}^{(d)} \otimes \mathcal{G}_{:,j_d}^{(d)} \rangle$ have been discussed after (18).

A. Summary of the algorithm

Algorithm 1 summarizes the proposed iterative algorithm. Since we have set the hyperparameters of the prior Gamma distributions $\{\alpha^{(d)}\}_{d=2}^D, \{\beta^{(d)}\}_{d=2}^D, \alpha_\tau, \beta_\tau$ to be 10^{-6} , the initialization of other variables can be set accordingly. In particular, the initialization of $\langle \lambda_k^{(d)} \rangle$ and $\langle \tau \rangle$ are set as $\alpha_k^{(d)} / \beta_k^{(d)} = 1$ and $\alpha_\tau / \beta_\tau = 1$, respectively. Consequently, the covariance of the TT-cores is initialized as $v_{\mathcal{G}_{k,\ell,:}^{(d)}} = \langle \lambda_k^{(d)} \rangle \langle \lambda_\ell^{(d+1)} \rangle I_{J_d} = I_{J_d}$. For the mean of the TT-cores,

we complete the observed tensor with random values drawn from $\mathcal{N}(0,1)$, decompose it using TT-SVD, and apply the results as the initialization. For the initial ranks, we adopt the maximal possible ranks $\mathbf{r}_{max} \in \mathbb{R}^{(D+1) \times 1}$, with its d -th element $(\mathbf{r}_{max})_d$ being the rank of the unfolding matrix $\mathbf{A}_{[d]} \in \mathbb{R}^{\prod_{d'=1}^{d-1} J_{d'} \times \prod_{d'=d+1}^D J_{d'}}$ [11], whose $[j_1 + \sum_{d'=2}^d (j_{d'} - 1) \prod_{i=1}^{d'-1} J_{d'-i}, j_{d+1} + \sum_{d'=d+2}^D (j_{d'} - 1) \prod_{i=1}^{d'-d-1} J_{d'-i}]$ -th element is the $[j_1, \dots, j_D]$ -th element in \mathcal{A}^1 . However, since the middle element of \mathbf{r}_{max} commonly grows exponentially with respect to the order of the tensor, which might be too big for high order tensor, we further set the upper bound of the initial TT rank to be 15 times the tensor dimension. Consequently, the initial TT rank is chosen as $L_d = \min((\mathbf{r}_{max})_d, 15J_d)$.

For the rank selection, as has been discussed after (18), slices of TT cores will be forced to be zero if $\lambda_k^{(d)}$ is big enough. Therefore, we can simply implement rank selection by eliminating slices with all-zero elements. Moreover, the pruning of all-zero slices can be done after each iteration, while not affecting the convergence of the algorithm, since every time when a slice is eliminated, it is equivalent to restarting the VI algorithm with a smaller model size and with the current variational distribution serving as a new initialization.

B. Complexity Analysis

The complexity of the proposed algorithm comes from the update of $\{\mathcal{G}^{(d)}\}_{d=1}^D$, $\{\lambda^{(d)}\}_{d=1}^D$ and τ . For simplicity, we suppose that all TT-ranks are initially set as L . For updating of each TT core $\mathcal{G}^{(d)}$, it takes $\mathcal{O}(2|\Omega|DL^2)$ to get $\mathbf{t}^{(<d)}$ and $\mathbf{t}^{(>d)}$, $\mathcal{O}(3|\Omega|DL^4)$ to get $\mathbf{b}^{(<d)}$ and $\mathbf{b}^{(>d)}$, then $\mathcal{O}(3|\Omega|J_dL^2)$ to get the variance and $\mathcal{O}(3|\Omega|J_dL^4)$ to get the mean in (17) and (18) respectively. Furthermore, each $\lambda^{(d)}$ requires $\mathcal{O}((J_d + J_{d-1})L^2)$ to compute, and τ requires $\mathcal{O}(|\Omega|(L^4 + L^2))$ to compute. It can be seen that the complexity is dominated by computing $\{\mathcal{G}^{(d)}\}_{d=1}^D$, and the overall complexity is $\mathcal{O}((\sum_{d=1}^D J_d + D^2)|\Omega|(L^2 + L^4))$, which could be large if the initial TT ranks are large. However it should be noticed that all-zero slices in TT cores can be pruned out after each iteration of the algorithm, thus the computational burden at later iterations would be smaller, especially for tensors with low true TT-ranks.

IV. NUMERICAL RESULTS ON SYNTHETIC AND REAL-WORLD DATA

A. Validation on Synthetic Data

We first test the capability of the proposed algorithm to estimate the TT-ranks. A synthetic tensor $\mathcal{Y} = \llbracket \mathcal{G}^{(1)}, \mathcal{G}^{(2)}, \mathcal{G}^{(3)} \rrbracket$ with size $[20, 20, 20]$ is considered, where each element of $\mathcal{G}^{(d)} \in \mathbb{R}^{R_d \times R_{d+1} \times 20}$ is drawn from a normal distribution $\mathcal{N}(0,1)$. Since the synthetic tensors are of order 3 and $R_1 = R_4 = 1$, we only need to determine the second and third TT-ranks. The original tensor is contaminated by additive

¹The mapping is the same as $\mathbf{A}_{[d]} = \text{reshape}(\mathcal{A}, \prod_{d'=1}^d J_{d'}, \prod_{d'=d+1}^D J_{d'})$ in MATLAB[®]

Algorithm 1 VI algorithm for the probabilistic TT-decomposition model

Initialization:

Input the observed tensor \mathcal{A} . Set initial ranks $\{L_d\}_{d=1}^D$ and hyperparameters $\{\alpha^{(d)}\}_{d=2}^D, \{\beta^{(d)}\}_{d=2}^D, \alpha_\tau, \beta_\tau$. Initialize $\{\langle \lambda^{(d)} \rangle\}_{d=1}^{D+1}, \langle \tau \rangle, \{\langle \mathcal{G}^{(d)} \rangle\}_{d=1}^D$ and $v_{\mathcal{G}_{k,\ell}^{(d)}}$ for $k = [1 : L_d]$, $\ell = [1 : L_{d+1}]$ and $d = [1 : D]$.

repeat

update $\{q(\mathcal{G}^{(d)})\}$:

for $d = 1$ to D do

$$\langle \mathbf{t}^{(<d)} \rangle = \langle \mathcal{G}_{\dots, j_1}^{(1)} \rangle \dots \langle \mathcal{G}_{\dots, j_{d-1}}^{(d-1)} \rangle$$

$$\langle \mathbf{t}^{(>d)} \rangle = \langle \mathcal{G}_{\dots, j_{d+1}}^{(d+1)} \rangle \dots \langle \mathcal{G}_{\dots, j_D}^{(D)} \rangle$$

$$\langle \mathbf{b}^{(<d)} \rangle = \langle \mathcal{G}_{\dots, j_1}^{(1)} \otimes \mathcal{G}_{\dots, j_1}^{(1)} \rangle \dots \langle \mathcal{G}_{\dots, j_{d-1}}^{(d-1)} \otimes \mathcal{G}_{\dots, j_{d-1}}^{(d-1)} \rangle$$

$$\langle \mathbf{b}^{(>d)} \rangle = \langle \mathcal{G}_{\dots, j_{d+1}}^{(d+1)} \otimes \mathcal{G}_{\dots, j_{d+1}}^{(d+1)} \rangle \dots \langle \mathcal{G}_{\dots, j_D}^{(D)} \otimes \mathcal{G}_{\dots, j_D}^{(D)} \rangle$$

for $k = 1$ to L_d do

for $\ell = 1$ to L_{d+1} do

update $v_{\mathcal{G}_{k,\ell}^{(d)}}$ as (18)

update $m_{\mathcal{G}_{k,\ell}^{(d)}}$ as (17)

end for

end for

end for

update $\{q(\lambda^{(d)})\}$:

for $d = 2$ to D do

$$\langle \lambda^{(d)} \rangle = [\hat{\alpha}_1^{(d)} / \hat{\beta}_1^{(d)}, \dots, \hat{\alpha}_{L_d}^{(d)} / \hat{\beta}_{L_d}^{(d)}] \text{ with } \hat{\alpha}_k^{(d)} \text{ in (21)}$$

$$\text{and } \hat{\beta}_k^{(d)} \text{ in (22)}$$

end for

update $q(\tau)$:

$$\langle \tau \rangle = \hat{\alpha}_\tau / \hat{\beta}_\tau \text{ with } \hat{\alpha}_\tau \text{ in (24) and } \hat{\beta}_\tau \text{ in (25)}$$

until convergence

Gaussian noise tensor \mathcal{W} , with $\mathcal{W}_{j_1 j_2 j_3} \sim \mathcal{N}(0, \sigma^2)$. The observed tensor is $\mathcal{A} = \mathcal{O} \circ (\mathcal{Y} + \mathcal{W})$, where \mathcal{O} is an indicator tensor with its elements drawn from the binomial distribution with certain missing rate. The performance of the proposed probabilistic TT model is tested under different signal-to-noise ratios (SNR) defined as $20 \log(\|\mathcal{A}\|_F / \|\mathcal{W}\|_F)$, missing ratios and true TT-ranks. Each testing condition is simulated for 100 times. The results are presented in bar figures with the average estimated TT-ranks represented by the heights of the bars, and a pair of lines showing the one standard deviation. Furthermore, the estimation accuracy is also shown on the top of each figure.

Fig. 5a shows the TT ranks estimation results under different missing rates. The true TT ranks are set as $[1, 5, 5, 1]$, and the SNR is set as 20dB. It can be seen that the estimation accuracy is higher than 90% in all cases, and achieves 100% when missing rate is equal or less than 20%. When the accuracy is not 100%, the standard deviation becomes larger as the missing rate becomes higher. The reason is that under higher missing rate, when the rank estimation goes wrong, it would give a rank that differs a lot from 5, like 20, while under lower missing rate, the wrongly estimated rank is commonly around the true rank 5.

Fig. 5b shows the rank accuracy under different SNRs, with the true TT ranks $[1, 5, 5, 1]$ and missing rate 0%. It is observed

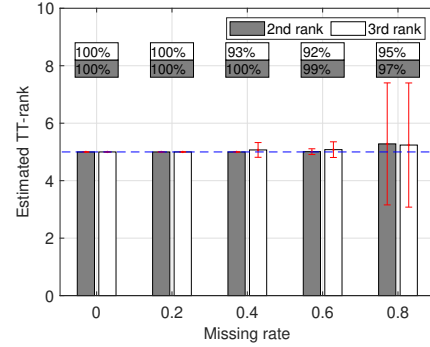
that when the SNR is equal or larger than 5dB, the rank accuracy is 100%. However, when the SNR becomes 0dB, the proposed method fails to give accurate estimation of the TT ranks, which is understandable as the strong noise masks the underlying TT structure.

Fig. 5c shows the estimated rank accuracy under different true TT ranks, with the missing rate set as 20% and the SNR set as 20dB. When the true TT ranks are $[1, 5, 5, 1]$ and $[1, 10, 10, 1]$, the proposed method gives 100% accuracy. When the TT ranks are set as $[1, 15, 15, 1]$ and $[1, 20, 20, 1]$, the estimation accuracy becomes lower, and generally the estimated ranks are smaller than the true ranks. The same phenomenon was also observed in Bayesian matrix decomposition [25] and CPD [21], and the reason might be the strong sparsity promoting property of the Gaussian-Gamma model, and the adopted Gaussian-product-Gamma model inherits such property.

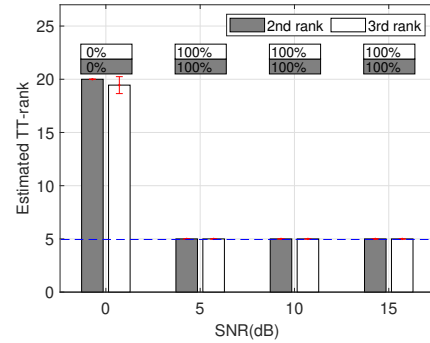
Next, we examine the tensor recovery ability using synthetic data, where Table I shows the relative standard error (RSE) of the recovered tensor $\hat{\mathcal{A}}$: $\|\mathcal{A} - \hat{\mathcal{A}}\|_F / \|\mathcal{A}\|_F$. In particular, the effects of the missing rate (with SNR = 20dB, TT ranks = $[1, 5, 5, 1]$), SNR (with 0% missing rate, TT ranks = $[1, 5, 5, 1]$), and the true TT ranks (with 20% missing rate, SNR = 20dB) are shown in Table Ia, Ib and Ic respectively. The results of the proposed method is compared with those of sparse tensor-train optimization (STTO) [4], simple low-rank tensor completion via TT (SiLRTC-TT) [2], tensor completion by parallel matrix factorization via TT (TMAC-TT) [2] and TT-SVD [11]. In addition, the tensor recovery performance of a non-TT-format tensor completion method - fully Bayesian CP factorization (FBCP) [3] is also compared. The tuning parameters of the above algorithms have been finely tuned to achieve the best performance. In particular, they are set as follows:

- For STTO, the TT rank parameters are set as $[1, 5, 5, 1]$.
- For SiLRTC-TT, the weighting parameters $\{\alpha_k\}_{k=1}^{D-1}$ are set as $\alpha_k = \delta_k / \sum_{k=1}^{D-1} \delta_k$ with $\delta_k = \min(\prod_{\ell=1}^k J_\ell, \prod_{\ell=k+1}^D J_\ell)$, and the parameters $\{\beta_k\}_{k=1}^{D-1}$ are set as $\beta_k = f\alpha_k$ with f being 0.5, as recommended in [2].
- For TMAC-TT, the weighting parameters $\alpha_k = \delta_k / \sum_{k=1}^{D-1} \delta_k$ are set in the same as in SiLRTC-TT, and the initial ranks $\{r_i\}_{i=1}^{D-1}$ are the number of components with singular values satisfying $\lambda_j^{[i]} / \lambda_{max}^{[i]} > 0.5$.
- For TT-SVD, the tolerance error is set as 0.
- For FBCP, the top-level hyperparameters c_0 , d_0 , a_0 and b_0 are all set to 10^{-6} , as recommended in [3]. The initial CP rank is set as the maximum of the tensor size $R = \max_{k=1}^D J_k$, and the factor matrices are initialized randomly.

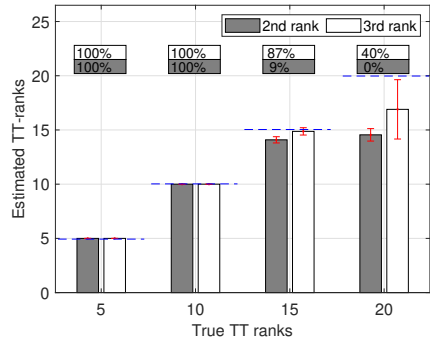
From Table I, it can be seen that the proposed method outperforms other methods in all cases. In particular, TT-SVD is not applicable when there are missing entries, as shown in Table Ia, while STTO, SiLRTC-TT, and TMAC-TT perform poorly when there is noise, as shown in Table Ib. For STTO, when there is little noise and the true ranks match its rank parameters, its performance is better than other optimization-



(a) with respect to missing rate (SNR = 20dB, true TT ranks = $[1, 5, 5, 1]$)



(b) with respect to SNR (0% missing rate, true TT ranks = $[1, 5, 5, 1]$)



(c) with respect to the true TT-ranks (20% missing rate, SNR = 20dB)

Fig. 5: Performance of rank estimation under different conditions.

based TT methods (i.e., SiLRTC-TT and TMAC-TT), but is still not as good as the performance of the proposed method, as Table Ia shows. On the other hand, when the true ranks are different from its rank parameters, STTO performs much worse than other methods, as shown in Table Ic. Finally, for FBCP, its performance is poor when the missing rate is high or the TT ranks are high, which is due to the mismatch between the assumed CPD format in FBCP and the more complicated TT structure in the synthetic data.

B. Image Completion

In this subsection, the results of image completion experiments on 13 images are presented, with the performance of

| missing rate | 0% | 20% | 40% | 60% | 80% |
|-----------------|----------------|----------------|----------------|----------------|----------------|
| proposed method | 8.22e-4 | 1.10e-3 | 1.50e-3 | 2.60e-3 | 4.12e-2 |
| STTO | 1.00e-2 | 8.30e-3 | 6.90e-3 | 6.00e-3 | 6.89e-2 |
| SiLRTC-TT | 1.00e-2 | 1.00e-2 | 1.58e-2 | 7.38e-2 | 5.27e-1 |
| TMAC-TT | 1.00e-2 | 1.63e-2 | 2.44e-2 | 1.26e-2 | 5.45e-1 |
| FBCP | 2.20e-3 | 2.60e-3 | 4.00e-3 | 7.60e-3 | 3.26e-1 |
| TT-SVD | 9.80e-3 | | | | Not applicable |

(a) with respect to the missing rate (SNR = 20dB, true TT ranks = [1, 5, 5, 1])

| SNR\dB | 0 | 5 | 10 | 15 |
|-----------------|----------------|----------------|----------------|----------------|
| proposed method | 7.90e-2 | 2.52e-2 | 8.10e-3 | 2.60e-3 |
| STTO | 1.01 | 3.17e-1 | 1.00e-1 | 3.12e-2 |
| SiLRTC-TT | 1.00 | 3.16e-1 | 1.00e-1 | 3.16e-2 |
| TMAC-TT | 1.00 | 3.17e-1 | 1.00e-1 | 3.16e-2 |
| FBCP | 1.77e-1 | 5.95e-2 | 2.06e-2 | 7.00e-3 |
| TT-SVD | 1.01 | 3.21e-1 | 9.90e-2 | 3.11e-2 |

(b) with respect to SNR (0% missing rate, true TT ranks = [1, 5, 5, 1])

| True TT ranks | 5 | 10 | 15 | 20 |
|-----------------|----------------|----------------|----------------|----------------|
| proposed method | 1.01e-3 | 3.90e-3 | 1.38e-2 | 7.40e-2 |
| STTO | 8.30e-3 | 9.83e-2 | 1.57e-1 | 1.63e-1 |
| SiLRTC-TT | 1.00e-2 | 1.90e-2 | 5.33e-2 | 9.17e-2 |
| TMAC-TT | 1.63e-2 | 4.62e-2 | 6.96e-2 | 8.32e-2 |
| FBCP | 2.60e-3 | 1.07e-2 | 1.11e-1 | 1.97e-1 |
| TT-SVD | | | | Not applicable |

(c) with respect to TT ranks (20% missing rate, SNR = 20dB)

TABLE I: RSE = $\|\mathcal{A} - \hat{\mathcal{A}}\|_F / \|\mathcal{A}\|_F$ of tensor recovery from incomplete and noisy observed tensors

the proposed algorithm compared with those of SiLRTC-TT [2], TMAC-TT [2], STTO [4], TTC-TV [26], FBCP [3], and FaLRTC [1]. The parameter settings of the algorithms are as follows:

- For STTO, the original images with size $256 \times 256 \times 3$ are folded into 9-dimensional tensors with size $4 \times 4 \times 3$, using tensor augmentation (will be introduced in the next paragraph), and the TT rank parameters are set as [1, 4, 12, 12, 12, 12, 12, 12, 3, 1].
- For SiLRTC-TT and TMAC-TT, the parameter settings are the same as that in IV-A, except that the initial rank parameters for TMAC-TT are the number of components with the singular values satisfying $\lambda_j^{[i]} / \lambda_{max}^{[i]} > 0.02$. Before adopting these algorithms, the original images are folded into size $4 \times 4 \times 3$ using tensor augmentation.
- For TTC-TV, the tensor dimension is factorized into $4 \times 8 \times 8 \times 8 \times 8 \times 4 \times 3$ in the way demonstrated in [26], and the TT rank parameters are set as [1, 4, 18, 18, 18, 12, 3, 1]. The regularization parameters for the total variance terms are $\lambda_1 = 0.2$, $\lambda_2 = 0.2$, and the scaling parameter for the box shaped interpolation kernel is $h = 22$.
- For FBCP, the parameter settings are the same as those in Section IV-A.
- For FaLRTC, the coefficients of the objective function are set as $\alpha = [1, 1, 10^{-3}]$, and the relaxation parameters are set as $[5/256, 5/256, 5 \times 10^{-3}/3]$.

For each image, Gaussian noise is added (with levels of noise specified in the result tables), and then 80 percents of the pixels

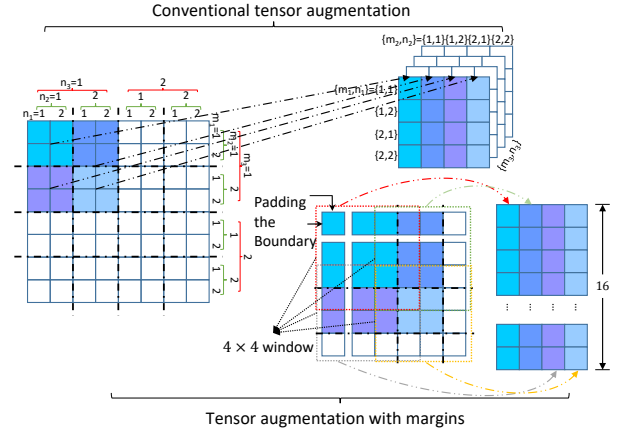


Fig. 6: Illustrations on tensor augmentation.

are randomly removed.

Before performing image completion, we adopt the tensor augmentation on the images, which is firstly introduced in [27], and further proved to be effective in image completions in [2]. The core concept of tensor augmentation is to fold a matrix into a high-order tensor. In particular, given a matrix $\mathbf{A} \in \mathbb{R}^{M \times N}$, its dimension M and N can be written as $M = \prod_{i=1}^f M_i$ and $N = \prod_{i=1}^f N_i$ for some integers $\{M_i\}$ and $\{N_i\}$. Then, we construct a tensor with elements $\mathcal{A}_{(M_1 N_1), (M_2 N_2), \dots, (M_f N_f)} = \mathbf{A}_{M_1 M_2 \dots M_f, N_1 N_2 \dots N_f}$, and finally get an f -th order tensor $\mathcal{A} \in \mathbb{R}^{M_1 N_1 \times M_2 N_2 \times \dots \times M_f N_f}$. Tensor augmentation is equivalent to have the original matrix

TABLE II: Performance of image completion without noise

| | Proposed Algorithm | SiLRTC-TT | TMAC-TT | STTO | TTC-TV | FBCP | FaLRTC |
|------------|--------------------|-------------|--------------------|-------------|-------------|--------------------|--------------------|
| | PSNR SSIM | PSNR SSIM | PSNR SSIM | PSNR SSIM | PSNR SSIM | PSNR SSIM | PSNR SSIM |
| airplane | 26.18 0.829 | 22.26 0.734 | 22.86 0.763 | 21.78 0.588 | 22.09 0.674 | 22.44 0.611 | 22.02 0.677 |
| baboon | 21.30 0.504 | 20.94 0.541 | 21.60 0.587 | 20.31 0.475 | 21.17 0.529 | 20.16 0.386 | 20.47 0.512 |
| barbara | 26.37 0.789 | 23.50 0.725 | 25.17 0.786 | 22.21 0.617 | 22.76 0.655 | 22.50 0.611 | 22.61 0.674 |
| couple | 29.22 0.852 | 26.01 0.765 | 28.12 0.851 | 26.57 0.728 | 26.40 0.736 | 27.06 0.732 | 26.40 0.770 |
| facade | 25.10 0.781 | 22.08 0.660 | 24.39 0.769 | 21.44 0.626 | 24.16 0.750 | 27.91 0.872 | 27.58 0.878 |
| goldhill | 26.09 0.745 | 23.45 0.657 | 25.35 0.737 | 22.99 0.595 | 23.09 0.631 | 23.40 0.596 | 23.30 0.656 |
| house | 28.95 0.824 | 24.53 0.774 | 26.00 0.791 | 24.06 0.634 | 24.55 0.722 | 24.23 0.685 | 24.33 0.743 |
| jellybeans | 30.48 0.941 | 25.00 0.872 | 25.28 0.884 | 24.93 0.735 | 25.44 0.877 | 23.50 0.831 | 25.17 0.885 |
| lena | 27.64 0.825 | 24.40 0.749 | 25.87 0.790 | 23.75 0.638 | 23.39 0.646 | 23.28 0.600 | 23.12 0.663 |
| peppers | 25.78 0.815 | 22.25 0.733 | 24.03 0.798 | 20.83 0.582 | 21.09 0.627 | 20.48 0.558 | 20.83 0.606 |
| sailboat | 23.62 0.723 | 20.78 0.663 | 22.93 0.750 | 20.23 0.554 | 20.81 0.610 | 20.82 0.550 | 20.65 0.627 |
| splash | 28.24 0.808 | 24.33 0.775 | 26.38 0.801 | 24.44 0.717 | 24.62 0.739 | 24.92 0.709 | 24.78 0.764 |
| tree | 24.12 0.734 | 20.93 0.657 | 23.12 0.734 | 20.43 0.541 | 20.35 0.584 | 19.70 0.482 | 20.29 0.575 |

TABLE III: Performance of image completion under Gaussian noise with variance 0.1

| | Proposed Algorithm | SiLRTC-TT | TMAC-TT | STTO | TTC-TV | FBCP | FaLRTC |
|------------|--------------------|-------------|-------------|-------------|-------------|--------------------|-------------|
| | PSNR SSIM | PSNR SSIM | PSNR SSIM | PSNR SSIM | PSNR SSIM | PSNR SSIM | PSNR SSIM |
| airplane | 18.51 0.452 | 14.13 0.181 | 10.49 0.078 | 15.11 0.207 | 15.00 0.224 | 16.57 0.218 | 13.50 0.163 |
| baboon | 18.56 0.276 | 14.76 0.193 | 10.52 0.091 | 15.35 0.209 | 15.23 0.218 | 16.67 0.180 | 14.00 0.170 |
| barbara | 18.98 0.409 | 14.85 0.183 | 10.60 0.073 | 15.45 0.204 | 15.42 0.235 | 16.60 0.239 | 13.92 0.162 |
| couple | 19.00 0.341 | 16.76 0.153 | 12.80 0.058 | 16.11 0.137 | 16.23 0.174 | 18.14 0.239 | 16.10 0.139 |
| facade | 18.76 0.295 | 14.91 0.203 | 11.56 0.112 | 15.33 0.222 | 15.58 0.318 | 19.47 0.471 | 15.21 0.323 |
| goldhill | 19.66 0.361 | 15.32 0.178 | 11.27 0.075 | 15.59 0.190 | 15.57 0.222 | 17.76 0.254 | 14.55 0.165 |
| house | 19.97 0.502 | 14.92 0.155 | 10.20 0.058 | 15.83 0.176 | 15.57 0.195 | 17.41 0.257 | 14.09 0.136 |
| jellybeans | 20.31 0.675 | 14.23 0.150 | 10.07 0.055 | 14.88 0.166 | 14.83 0.176 | 18.11 0.334 | 13.68 0.133 |
| lena | 19.72 0.464 | 15.07 0.176 | 11.05 0.067 | 15.58 0.181 | 15.64 0.208 | 16.99 0.233 | 14.08 0.152 |
| peppers | 17.76 0.432 | 14.04 0.182 | 9.63 0.061 | 14.51 0.205 | 14.85 0.228 | 15.09 0.215 | 12.94 0.149 |
| sailboat | 17.38 0.358 | 14.04 0.200 | 9.14 0.078 | 14.91 0.232 | 15.04 0.266 | 15.95 0.255 | 13.68 0.202 |
| splash | 19.11 0.449 | 15.14 0.172 | 10.45 0.057 | 16.11 0.204 | 15.96 0.209 | 18.04 0.307 | 14.92 0.172 |
| tree | 17.41 0.361 | 13.99 0.211 | 9.19 0.075 | 14.88 0.242 | 15.04 0.274 | 15.36 0.208 | 13.23 0.182 |

TABLE IV: Average run time over 26 images

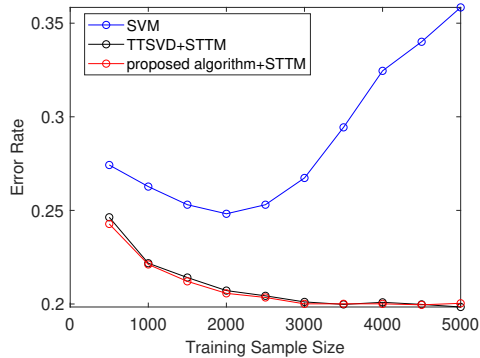
| | Proposed Algorithm | SiLRTC-TT | TMAC-TT | STTO | TTC-TV | FBCP | FaLRTC |
|-------------------|--------------------|-----------|---------|--------|--------|-------|--------|
| average runtime\s | 732.99 | 25.73 | 35.07 | 478.09 | 12.34 | 29.51 | 17.17 |

cut into multiple small matrix blocks, and then treat each matrix block as a fiber of the reordered tensor. An example of tensor augmentation is illustrated in the upper part of Fig. 6. In our experiments, we further improve the tensor augmentation by padding the images and using overlapping windows, which is shown in the bottom part of Fig. 6. In particular, the boundaries of the image is first replicated. Then, instead of folding the basic 2×2 matrix block, overlapping 4×4 matrix blocks (with stride 2) is folded as columns of the new tensor. The reason for doing so is that the neighbourhood information of the separated matrix blocks will be retained after reordering the entries. In the experiments, we add boundary padding to the original image of size $2^8 \times 2^8 \times 3$, and then reshape it to a 9-dimensional tensor with size $16 \times 4 \times 3$.

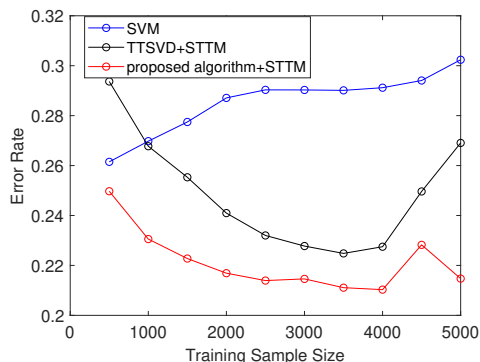
Table II and Table III show the peak signal-to-noise ratio (PSNR) $20 \ln(\max(\mathbf{A})\sqrt{3MN}/\|\mathbf{A} - \hat{\mathbf{A}}\|_F)$ and the structural similarity index measure (SSIM) [28] of the recovered images under no noise and under Gaussian noise with variance 0.1, respectively. It can be seen that the proposed algorithm achieves the overall best performance in terms of both PSNR and SSIM, no matter there is noise or not. When there is no noise, in most cases the proposed algorithm recovers images with more than 1dB higher PSNR than other algorithms. Furthermore, for the 'airplane' and 'jellybeans' figures, the improvement is over 3dB and 5dB in PSNR respectively compared to the second best, and the better PSNR is also visually evident in the recovered images shown in Fig. 7. When there is Gaussian noise with variance 0.1, the performance of the



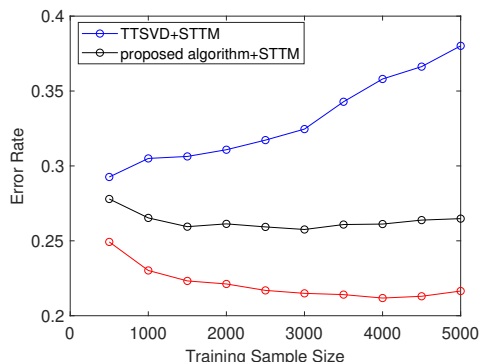
Fig. 7: Visual effects of the image completion experiments, from top to bottom: (1) original images; (2) images with 80% missing data and without noise; (3) recovered images from 80% missing data through: the proposed algorithm, SiLRTC-TT, TMAC-TT, STTO, TTC-TV, FBCP, FaLRTC, respectively; (4) images with 80% missing data under Gaussian noise with variance 0.1; (5) recovered images from 80% missing data and Gaussian noise with variance 0.1 through: the proposed algorithm, SiLRTC-TT, TMAC-TT, STTO, TTC-TV, FBCP, FaLRTC, respectively.



(a) Training and testing on clean data



(b) Training and testing on noisy data



(c) Training using clean data and testing on noisy data

Fig. 8: Testing Accuracy with respect to training size.

proposed algorithm achieves about 2dB higher PSNR and more than 0.1 higher SSIM than the second best, and recovers recognizable figures as shown in Fig. 7. One thing worth to note is that SILRTC-TT, TMAC-TT and FaLRTC all set $\hat{\mathbf{A}} = \mathbf{A}$ as a constraint in their optimization schemes. Thus, they inherently cannot handle noisy data, and this is clearly corroborated in the poorly recovered images in Fig. 7.

Table IV shows the average runtime of various algorithms for the tested incomplete images, with the testing environment being MATLAB2018b on a desktop computer with an Intel i7 six-core processor at 3.7GHz and 16GB RAM. On the surface, it might seem that the proposed algorithm take more time to recover the images, but it is important to recognize that the proposed algorithm does not require any parameter tuning, and it automatically balances the model complexity

and avoidance of noise overfitting. Given the small runtime of other algorithms, one may contemplate tuning the parameters to improve their performance. However, such a strategy is not practical as computing PSNR and SSIM requires the ground truth image, which is not available in practical applications. Even if we could come up with a tuning objective without the ground truth, the exhaustive tuning may eventually end up with longer runtime than the proposed algorithm. Take the most time efficient algorithm TTC-TV as an example, there are at least 5 parameters (corresponding to the ranks of the tensor cores, regularization terms and the scaling parameter) that need to be fine-tuned. Even if each parameter is tested for only 10 different values, the overall computation time will be 10^5 times the average runtime in Table IV. From this perspective, the proposed algorithm provides an economical complexity while achieving automatic model selection.

C. Image Classification

In this subsection, we test the performance of the proposed algorithm on image classification. In particular, after the TT decomposition, the TT cores of the decomposed data are fed into the support tensor train machine (STTM) [7], which extends the support vector machine (SVM) to tensors and adopts TT-structured weighting parameters for classification. The original STTM uses TT-SVD to decompose the data for training and testing, while in our experiments the proposed algorithm is adopted. Additionally, the performance of SVM is also tested for comparison. The cifar-10 dataset [29] is used in the experiments, from which different sample sizes are used for training (specified in Fig. 8) and 1000 images are used for testing. Three scenarios are considered: clean data for training and testing, noisy data for training and testing, training on clean data and testing on noisy data. Gaussian noise with zero mean and variance 0.01 is added to generate the noisy data. Since both STTM and SVM are binary classifiers, but there are totally 10 classes in the dataset, we perform classification for every two classes, and calculate the average error rate.

The results of the classification are presented in Fig. 8. From Fig. 8a it can be seen that for the clean data, STTM combined with TT-SVD and the proposed algorithm achieve similar performance, under all training sample sizes, and both outperform SVM. However, as illustrated in Fig. 8b and 8c, when there is noise, no matter in both training and testing data, or in only the testing data, STTM combined with TT-SVD performs much worse than the proposed algorithm. This is because that the proposed algorithm can recover the underlying TT structure of the data even under noise perturbation, while TT-SVD cannot.

V. CONCLUSIONS

In this paper, a probabilistic TT model, with the capability of automatic rank determination was proposed. The legitimacy of the proposed model was verified by establishing the sparsity promoting property of the adopted Gaussian-product-Gamma prior. Learning algorithm was derived under variational inference framework. Simulation results on synthetic data demonstrated the ability of the proposed algorithm to accurately

recover the underlying TT structure from incomplete noisy data. Furthermore, experiments on image completion and image classification showed the proposed algorithm leads to higher recovery or classification accuracy than other state-of-the-art TT decomposition algorithms.

APPENDIX A

PROPERTIES OF THE GAUSSIAN-PRODUCT-GAMMA MODEL

With the model in (3), the joint distribution is given by:

$$\begin{aligned}
P(x, \lambda_1, \lambda_2 | \alpha_1, \beta_1, \alpha_2, \beta_2) &= \mathcal{N}(x|0, (\lambda_1 \lambda_2)^{-1}) \text{Gamma}(\lambda_1 | \alpha_1, \beta_1) \text{Gamma}(\lambda_2 | \alpha_2, \beta_2) \\
&= \frac{\beta_1^{\alpha_1} \beta_2^{\alpha_2}}{\sqrt{2\pi} \Gamma(\alpha_1) \Gamma(\alpha_2)} \lambda_1^{\alpha_1 - \frac{1}{2}} \lambda_2^{\alpha_2 - \frac{1}{2}} \\
&\quad \times \exp\left\{-\left(\frac{\lambda_1 \lambda_2}{2} x^2 + \beta_1 \lambda_1 + \beta_2 \lambda_2\right)\right\}.
\end{aligned} \tag{26}$$

Integrating out λ_1 , then the joint distribution of x and λ_2 can be obtained,

$$\begin{aligned}
P(x, \lambda_2 | \alpha_1, \beta_1, \alpha_2, \beta_2) &= \frac{\beta_1^{\alpha_1} \beta_2^{\alpha_2} \lambda_2^{\alpha_2 - \frac{1}{2}}}{\sqrt{2\pi} \Gamma(\alpha_1) \Gamma(\alpha_2)} \exp\{-\beta_2 \lambda_2\} \\
&\quad \times \int \lambda_1^{\alpha_1 - \frac{1}{2}} \exp\left\{-\left(\frac{\lambda_2}{2} x^2 + \beta_1\right) \lambda_1\right\} d\lambda_1 \\
&= \frac{\beta_1^{\alpha_1} \beta_2^{\alpha_2} \lambda_2^{\alpha_2 - \frac{1}{2}} \Gamma(\alpha_1 + \frac{1}{2})}{\sqrt{2\pi} \Gamma(\alpha_1) \Gamma(\alpha_2)} \left(\frac{\lambda_2}{2} x^2 + \beta_1\right)^{-(\alpha_1 + \frac{1}{2})} \\
&\quad \times \exp\{-\beta_2 \lambda_2\}.
\end{aligned} \tag{27}$$

The integration is calculated by observing that the factors to be integrated is an unnormalized Gamma distribution with $\alpha' = \alpha_1 + \frac{1}{2}$ and $\beta' = \frac{\lambda_2}{2} x^2 + \beta_1$. Divide (26) by (27), then the conditional posterior distribution of λ_1 is obtained:

$$\begin{aligned}
P(\lambda_1 | x, \lambda_2, \alpha_1, \beta_1, \alpha_2, \beta_2) &= \frac{P(x, \lambda_1, \lambda_2 | \alpha_1, \beta_1, \alpha_2, \beta_2)}{P(x, \lambda_2 | \alpha_1, \beta_1, \alpha_2, \beta_2)} \\
&= \frac{1}{\Gamma(\alpha_1 + \frac{1}{2})} \left(\frac{\lambda_2}{2} x^2 + \beta_1\right)^{\alpha_1 + \frac{1}{2}} \lambda_1^{\alpha_1 - \frac{1}{2}} \\
&\quad \times \exp\left\{-\left(\frac{\lambda_2}{2} x^2 + \beta_1\right) \lambda_1\right\}.
\end{aligned} \tag{28}$$

It can be seen that the conditional distribution of λ_1 is still a Gamma distribution, more exactly, $\text{Gamma}(\alpha_1 + \frac{1}{2}, \frac{\lambda_2}{2} x^2 + \beta_1)$. The proof of the conditional posterior of λ_2 is similar with that of λ_1 .

For the marginal distribution of x , we need to further integrate out λ_2 in (27):

$$\begin{aligned}
P(x | \alpha_1, \beta_1, \alpha_2, \beta_2) &= \int P(x, \lambda_2 | \alpha_1, \beta_1, \alpha_2, \beta_2) d\lambda_2 \\
&= \frac{\beta_1^{\alpha_1} \beta_2^{\alpha_2} \Gamma(\alpha_1 + \frac{1}{2})}{\sqrt{2\pi} \Gamma(\alpha_1) \Gamma(\alpha_2)} \int \lambda_2^{\alpha_2 - \frac{1}{2}} \left(\frac{x^2}{2} \lambda_2 + \beta_1\right)^{-(\alpha_1 + \frac{1}{2})} \\
&\quad \times \exp\{-\beta_2 \lambda_2\} d\lambda_2.
\end{aligned} \tag{29}$$

Since $\alpha_1 + \frac{1}{2} > 0$ and $\beta_1 > 0$, we have $(\frac{x^2}{2} \lambda_2 + \beta_1)^{-(\alpha_1 + \frac{1}{2})} \leq \beta_1^{-(\alpha_1 + \frac{1}{2})}$ when $\lambda_2 \in [0, \infty)$. Then because $\beta_1^{-(\alpha_1 + \frac{1}{2})} \int_0^\infty \lambda_2^{\alpha_2 - \frac{1}{2}} \exp\{-\beta_2 \lambda_2\} d\lambda_2$ converges, the integration in equation (29) converges.

APPENDIX B

SPARSITY OF THE PROBABILISTIC TT MODEL

To prove that (8) and (9) would induce sparsity, we need to prove that the marginal prior distribution $p(\mathcal{G}_{k, :, :}^{(d)})$ and $p(\mathcal{G}_{:, \ell, :}^{(d)})$ are sparsity promoting. Below, we focus on $p(\mathcal{G}_{k, :, :}^{(d)})$ as the logic for $p(\mathcal{G}_{:, \ell, :}^{(d)})$ is the same. To get its marginal prior distribution, we first obtain $p(\mathcal{G}_{k, :, :}^{(d)}, \lambda_k^{(d)}, \lambda^{(d+1)})$ by picking up relevant factors from the product of (8) and (9), which is

$$\begin{aligned}
p(\mathcal{G}_{k, :, :}^{(d)}, \lambda_k^{(d)}, \lambda^{(d+1)}) &= \prod_{\ell}^{L_{d+1}} \left(\frac{\sqrt{\lambda_k^{(d)} \lambda_{\ell}^{(d+1)}}}{\sqrt{2\pi}}\right)^{J_d} \exp\left\{-\frac{\lambda_k^{(d)} \lambda_{\ell}^{(d+1)}}{2} \sum_{j_d} \mathcal{G}_{k, \ell, j_d}^{(d)2}\right\} \\
&\quad \times \frac{\beta_{\lambda_k}^{(d) \alpha_{\lambda_k}^{(d)}} \lambda_k^{(d) \alpha_{\lambda_k}^{(d)} - 1}}{\Gamma(\alpha_{\lambda_k}^{(d)})} \exp\left\{-\beta_{\lambda_k}^{(d)} \lambda_k^{(d)}\right\} \\
&\quad \times \prod_{\ell=1}^{L_{d+1}} \frac{\beta_{\lambda_{\ell}}^{(d+1) \alpha_{\lambda_{\ell}}^{(d+1)}} \lambda_{\ell}^{(d+1) \alpha_{\lambda_{\ell}}^{(d+1)} - 1}}{\Gamma(\alpha_{\lambda_{\ell}}^{(d+1)})} \\
&\quad \times \exp\left\{-\beta_{\lambda_{\ell}}^{(d+1)} \lambda_{\ell}^{(d+1)}\right\}.
\end{aligned} \tag{30}$$

Next (30) is rewritten as

$$\begin{aligned}
p(\mathcal{G}_{k, :, :}^{(d)}, \lambda_k^{(d)}, \lambda^{(d+1)}) &\propto \lambda_k^{(d) \frac{J_d}{2} + \alpha_{\lambda_k}^{(d)} - 1} \exp\left\{-\beta_{\lambda_k}^{(d)} \lambda_k^{(d)}\right\} \\
&\quad \times \prod_{\ell=1}^{L_{d+1}} \lambda_{\ell}^{(d+1) \frac{J_d}{2} + \alpha_{\lambda_{\ell}}^{(d+1)} - 1} \\
&\quad \times \exp\left\{-\left(\frac{\lambda_k^{(d)} \sum_{j_d} \mathcal{G}_{k, \ell, j_d}^{(d)2}}{2} + \beta_{\lambda_{\ell}}^{(d+1)}\right) \lambda_{\ell}^{(d+1)}\right\}.
\end{aligned} \tag{31}$$

By observing that each $\lambda_{\ell}^{(d+1)}$ follows a Gamma distribution with a new set of hyperparameters, we can integrate out $\lambda_{\ell}^{(d+1)}$ and obtain

$$\begin{aligned}
p(\mathcal{G}_{k, :, :}^{(d)}, \lambda_k^{(d)}) &\propto \lambda_k^{(d) \frac{J_d}{2} + \alpha_{\lambda_k}^{(d)} - 1} \exp\left\{-\beta_{\lambda_k}^{(d)} \lambda_k^{(d)}\right\} \\
&\quad \times \prod_{\ell=1}^{L_{d+1}} \left(\frac{\lambda_k^{(d)} \sum_{j_d} \mathcal{G}_{k, \ell, j_d}^{(d)2}}{2} + \beta_{\lambda_{\ell}}^{(d+1)}\right)^{-(\frac{J_d}{2} + \alpha_{\lambda_{\ell}}^{(d+1)})}
\end{aligned} \tag{32}$$

With $\alpha_{\lambda_{\ell}}^{(d+1)}$ and $\beta_{\lambda_{\ell}}^{(d+1)}$ tend to zero, as $(\frac{\lambda_k^{(d)} \sum_{j_d} \mathcal{G}_{k, \ell, j_d}^{(d)2}}{2} + \beta_{\lambda_{\ell}}^{(d+1)})^{-(\frac{J_d}{2} + \alpha_{\lambda_{\ell}}^{(d+1)})}$ tends to $(\frac{\lambda_k^{(d)}}{2} \sum_{j_d} \mathcal{G}_{k, \ell, j_d}^{(d)2})^{-\frac{J_d}{2}}$, (32)

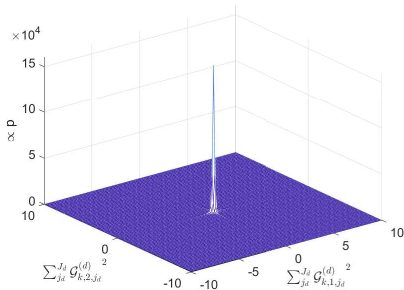


Fig. 9: model sparsity

becomes

$$\begin{aligned}
 & \lim_{\substack{\alpha_{\lambda}^{(d+1)} \rightarrow 0 \\ \beta_{\lambda}^{(d+1)} \rightarrow 0}} p(\mathcal{G}_{k, :, :}, \lambda_k^{(d)}) \\
 & \propto \lambda_k^{(d) \frac{J_d}{2}(1-L_{d+1}) + \alpha_{\lambda_k}^{(d)} - 1} \exp\left\{-\beta_{\lambda_k}^{(d)} \lambda_k^{(d)}\right\} \\
 & \times \prod_{\ell=1}^{L_{d+1}} \left(\sum_{j_d} \mathcal{G}_{k, \ell, j_d}^{(d) 2}\right)^{-\frac{J_d}{2}},
 \end{aligned} \quad (33)$$

in which the distribution of $\lambda_k^{(d)}$ and $\mathcal{G}_{k, :, :}^{(d)}$ can be separated, and thus we get

$$p(\mathcal{G}_{k, :, :}^{(d)}) \propto \prod_{\ell=1}^{L_{d+1}} \left(\sum_{j_d} \mathcal{G}_{k, \ell, j_d}^{(d) 2}\right)^{-\frac{J_d}{2}}. \quad (34)$$

The distribution of $\mathcal{G}_{k, :, :}^{(d)}$ will take very large value when the sum of squares of all $\mathcal{G}_{k, \ell, j_d}^{(d)}$, $\ell \in [1 : L_{d+1}]$ tend to zero. Thus the marginalized prior distribution (34) induces sparsity in the whole slice $\mathcal{G}_{k, :, :}^{(d)}$. A demonstration of (34) with $L_{d+1} = 2$ is shown in Fig. 9. It can be seen that most of the probability density concentrates in a region where $\sum_{j_d} \mathcal{G}_{k, 1, j_d}^{(d) 2}$ and $\sum_{j_d} \mathcal{G}_{k, 2, j_d}^{(d) 2}$ tend to zero. Similar conclusion can also be drawn under other L_{d+1} .

REFERENCES

- [1] J. Liu, P. Musialski, P. Wonka, and J. Ye, "Tensor completion for estimating missing values in visual data," *IEEE transactions on pattern analysis and machine intelligence*, vol. 35, no. 1, pp. 208–220, 2013.
- [2] J. A. Bengua, H. N. Phien, H. D. Tuan, and M. N. Do, "Efficient tensor completion for color image and video recovery: Low-rank tensor train," *IEEE Transactions on Image Processing*, vol. 26, no. 5, pp. 2466–2479, 2017.
- [3] Q. Zhao, L. Zhang, and A. Cichocki, "Bayesian cp factorization of incomplete tensors with automatic rank determination," *IEEE transactions on pattern analysis and machine intelligence*, vol. 37, no. 9, pp. 1751–1763, 2015.
- [4] L. Yuan, Q. Zhao, and J. Cao, "High-order tensor completion for data recovery via sparse tensor-train optimization," in *2018 IEEE international conference on acoustics, speech and signal processing (ICASSP)*. IEEE, 2018, pp. 1258–1262.
- [5] D. Tao, X. Li, W. Hu, S. Maybank, and X. Wu, "Supervised tensor learning," in *Fifth IEEE International Conference on Data Mining (ICDM'05)*. IEEE, 2005, pp. 8–pp.
- [6] I. Kotsia and I. Patras, "Support tucker machines," in *CVPR 2011*. IEEE, 2011, pp. 633–640.
- [7] C. Chen, K. Batselier, C.-Y. Ko, and N. Wong, "A support tensor train machine," in *2019 International Joint Conference on Neural Networks (IJCNN)*. IEEE, 2019, pp. 1–8.
- [8] Y.-D. Kim, E. Park, S. Yoo, T. Choi, L. Yang, and D. Shin, "Compression of deep convolutional neural networks for fast and low power mobile applications," *arXiv preprint arXiv:1511.06530*, 2015.
- [9] A. Novikov, D. Podoprikin, A. Osokin, and D. P. Vetrov, "Tensorizing neural networks," in *Advances in neural information processing systems*, 2015, pp. 442–450.
- [10] A. Tjandra, S. Sakti, and S. Nakamura, "Compressing recurrent neural network with tensor train," in *2017 International Joint Conference on Neural Networks (IJCNN)*. IEEE, 2017, pp. 4451–4458.
- [11] I. V. Oseledets, "Tensor-train decomposition," *SIAM Journal on Scientific Computing*, vol. 33, no. 5, pp. 2295–2317, 2011.
- [12] S. Holtz, T. Rohwedder, and R. Schneider, "The alternating linear scheme for tensor optimization in the tensor train format," *SIAM Journal on Scientific Computing*, vol. 34, no. 2, pp. A683–A713, 2012.
- [13] T. Rohwedder and A. Uschmajew, "On local convergence of alternating schemes for optimization of convex problems in the tensor train format," *SIAM Journal on Numerical Analysis*, vol. 51, no. 2, pp. 1134–1162, 2013.
- [14] L. Grasedyck, M. Kluge, and S. Krämer, "Alternating least squares tensor completion in the tt-format," *arXiv preprint arXiv:1509.00311*, 2015.
- [15] A.-H. Phan, A. Cichocki, A. Uschmajew, P. Tichavsky, G. Luta, and D. Mandic, "Tensor networks for latent variable analysis. part i: Algorithms for tensor train decomposition," *arXiv preprint arXiv:1609.09230*, 2016.
- [16] M. Imaizumi, T. Maehara, and K. Hayashi, "On tensor train rank minimization: Statistical efficiency and scalable algorithm," in *Advances in Neural Information Processing Systems*, 2017, pp. 3930–3939.
- [17] L. Cheng, Y.-C. Wu, and H. V. Poor, "Probabilistic tensor canonical polyadic decomposition with orthogonal factors," *IEEE Trans. Signal Processing*, vol. 65, no. 3, pp. 663–676, 2017.
- [18] Q. Zhao, L. Zhang, and A. Cichocki, "Bayesian sparse tucker models for dimension reduction and tensor completion," *arXiv preprint arXiv:1505.02343*, 2015.
- [19] C. Hawkins and Z. Zhang, "Bayesian tensorized neural networks with automatic rank selection," *arXiv preprint arXiv:1905.10478*, 2019.
- [20] C. M. Bishop, "Bayesian pca," in *Advances in neural information processing systems*, 1999, pp. 382–388.
- [21] L. Cheng, X. Tong, S. Wang, Y.-C. Wu, and H. V. Poor, "Learning nonnegative factors from tensor data: Probabilistic modeling and inference algorithm," *IEEE Transactions on Signal Processing*, vol. 68, pp. 1792–1806, 2020.
- [22] C. M. Bishop, *Pattern recognition and machine learning*. springer, 2006.
- [23] K. P. Murphy, "A probabilistic perspective," *Text book*, 2012.
- [24] C. Walck *et al.*, "Hand-book on statistical distributions for experimentalists," *University of Stockholm*, vol. 10, 2007.
- [25] L. Yang, J. Fang, H. Duan, H. Li, and B. Zeng, "Fast low-rank bayesian matrix completion with hierarchical gaussian prior models," *IEEE Transactions on Signal Processing*, vol. 66, no. 11, pp. 2804–2817, 2018.
- [26] C.-Y. Ko, K. Batselier, L. Daniel, W. Yu, and N. Wong, "Fast and accurate tensor completion with total variation regularized tensor trains," *IEEE Transactions on Image Processing*, 2020.
- [27] J. I. Latorre, "Image compression and entanglement," *arXiv preprint quant-ph/0510031*, 2005.
- [28] Z. Wang, A. C. Bovik, H. R. Sheikh, and E. P. Simoncelli, "Image quality assessment: from error visibility to structural similarity," *IEEE transactions on image processing*, vol. 13, no. 4, pp. 600–612, 2004.
- [29] A. Krizhevsky, G. Hinton *et al.*, "Learning multiple layers of features from tiny images," 2009.